# A method for generating quantitative vapor-phase infrared spectra of solids: results for phenol, camphor, menthol, syringol, dicyclopentadiene and naphthalene

Matthew D.W. Schneider, Tracy J. Baker, Nicole K. Scharko, Thomas A. Blake, Russell G. Tonkyn, Brenda M. Forland, Timothy J. Johnson *

*Pacific Northwest National Laboratory Richland, Washington 99352, USA*

ARTICLE INFO

*Keywords:*
Infrared
Solid vapor
Gas-phase spectra
FTIR
Database
Absorption coefficients
Dicyclopentadiene
Menthol
Syringol
Phenol
Camphor and naphthalene

ABSTRACT

A method is presented to generate quantitative vapor-phase infrared spectra from substances that naturally occur as solids with moderate volatility. The solid is gravimetrically dissolved into a solvent that has few infrared spectral features, typically $CS_2$ and $CCl_4$ separately. The solution is flowed at a constant rate from a linearly pumped syringe into a metered stream of nitrogen carrier gas regulated by a mass flow controller. The analyte/solvent mix is flash vaporized by volatilizing the solution across a heated stainless-steel surface as it emanates from the syringe tip. The $N_2$ gas-solution mixture is flowed into a long-path White cell thermostatted at a desired temperature, the long optical path compensating for the modest analyte mixing ratio. A composite spectrum is generated from typically ten or more 760-Torr pressure-broadened spectra over the 600 to 6500 $cm^{-1}$ spectral range at 0.1 $cm^{-1}$ spectral resolution. The solid analytes reported here using this novel technique include dicyclopentadiene, menthol, syringol, phenol, camphor, and naphthalene.

## 1. Introduction

The Pacific Northwest National Laboratory (PNNL) continues to deliver broadband quantitative infrared reference spectra for atmospheric sensing [1–5]. The data are versatile since the spectra may be used with both passive or active sources, and with either narrowband (e.g. laser) or broadband systems (e.g. a Fourier transform infrared spectrometer – FTIR) [6–10]. The spectra represent chemicals of various origins, including anthropogenic environmental pollutants, toxic industrial chemicals, compounds associated with energy production, biogenic sources, as well as chemicals whose vapors are linked to biomass burning plumes or toxic chemicals such as perfluoroalkyl substances (PFAS) [3,11–13] The spectra are unique in three regards: a) a high spectral resolution (0.11 $cm^{-1}$) is used with all data recorded as 760-Torr pressure broadened samples, b) the data have a large frequency range with a minimum span of 600 to 6500 $cm^{-1}$, and most importantly, c) the spectra are quantitative, corresponding to a pressure-pathlength burden of one part per million analyte concentration in one atmosphere of nitrogen over a pathlength of one meter at 296 K (1 ppm-m). The databases have found use in industrial, academic and remote sensing scenarios [14–16].

These databases have a gap, however, namely the absence of measured vapor-phase spectra for compounds that naturally occur as solids. In the early phases of the effort, most of the measurements [2,17] were made on a static system by either bleeding in gases or passively vaporizing high volatility liquids, accurately measuring their vapor pressures and quantifying the burden via the ideal gas law. Absorbances were calculated by using Beer's law over the fixed (20 cm) path length. The method worked extremely well for hundreds of species that exist either as gases or liquids of substantial vapor pressure. As a general guideline, typically ~1 Torr vapor pressure or greater at 25 °C is needed to use this method, but this value varies depending on the IR cross-sections, as well as other properties such as e.g. adhesion, dipole moment, chemical stability [18].

For liquids of lower volatility, the method was no longer reliable at generating quantitative gas-phase concentrations, and it was found necessary to make two adjustments: First, due to smaller concentrations, the optical path was increased by using a thermostatted long path White cell (typically set to 805 cm). The cell is also gold plated to accommodate many reactive compounds. Second, an alternative method was needed to

* Corresponding author.
*E-mail address:* timothy.johnson@pnnl.gov (T.J. Johnson).

generate reliable gas-phase concentrations. Rather than the passive vaporization system, PNNL developed and built a flow system patterned after the examples of Nelson et al. [19,20] and the methods of Kleimeyer and co-workers [21]. In the dynamic method, the liquid sample is volumetrically eluted from the tip of a syringe and evaporated into a metered stream of ultra-high purity nitrogen ($N_2$) carrier gas. The dynamic mixture equilibrates to a steady-state concentration and the infrared spectroscopic measurement is made on the flowed mixture. The PNNL method improved upon the method by having the liquid emanating from the syringe tip flow directly onto a sloped stainless-steel surface that is heated to an elevated temperature typically 20 to 40 °C below the liquid's boiling point. The sample is thus flash volatilized and diluted in the nitrogen stream that flows perpendicular across the syringe tip [22]. The disseminator-flow method allows generation of quantitative mixtures for liquids with vapor pressures as low as 0.01 to 0.001 Torr, again depending on the parameters listed above including surface adhesion and chemical stability, particularly for species containing functional groups such as thionyl groups or peroxides [18,23]. It is noted that the requisite long-path cells are typically of large volume and surface area, and thus any "cold spots" in the flow path lead to condensation, rendering an inaccurate partial pressure value. Specially designed gas cells in which the gas cell jacket has connections for circulation of heating or cooling liquid were constructed to redress this issue.

Similar to low volatility liquids, the greatest challenge for solids is generating quantitative vapor-phase mixing ratios. Despite the challenges, certain solid compounds are of sufficient interest to warrant vapor phase studies. Some of these compounds include those relevant to biomass burning [11,12,24], such as volatile organic compounds (VOCs), oxygenated volatile organic compounds (OVOCs), and polycyclic aromatic hydrocarbons (PAHs), etc. Many of these exist as solids (e.g. phenol, 4-vinylphenol, chloroacetic acid, butanedioic acid, etc.). Table 1 displays the solid analytes and solvents used in this study, as well as associated physical properties such as vapor pressures, most of which are intrinsically low. For example, naphthalene [2] has a vapor pressure of 0.083 Torr at 25 °C. Due to such low volatilities, it was necessary to develop an alternative method to reliably measure a quantitative infrared absorption spectrum of such compounds. Our approach is simply a quantitative dissolution of the solid of interest in an appropriate solvent, thus using a variant of the disseminator-flow system outlined above for liquids. Ideally, the solvent of choice would 1) dissolve all solutes of interest, 2) have a moderately high vapor pressure, and 3) be nearly transparent in the infrared. Highly symmetric species such as carbon tetrachloride ($CCl_4$) or carbon disulfide ($CS_2$) are good candidates. Carbon tetrachloride has long been appreciated for its few strong absorption bands in the fingerprint region, with multiple vendors offering "IR grade" versions for liquid-phase work. Similarly, $CS_2$ has few strong absorption features in the fingerprint region and, importantly, its bands do not overlap with those of $CCl_4$. In the best cases the target analyte has reasonable solubility in both.

Both $CS_2$ and $CCl_4$ have been employed as solvents in non-quantitative studies that report the IR spectra of liquid analytes that required dilution due to the analyte's large absorption cross sections, but also in a few cases for samples which are in fact solids at room temperature, including some of the compounds reported in this work. These prior non-quantitative works include, for example, naphthalene [25] dissolved in either $CS_2$ or $CCl_4$, menthol [26] in $CCl_4$, phenol [27] in $CS_2$, camphor [28] in $CCl_4$, and syringol in both $CS_2$ [29] and $CCl_4$ [30]. Interestingly, there is one study that reports the gas phase IR spectrum for SCSe (thiocarbonyl selenide) that contained residual amounts of $CS_2$, a reactant used for the preparation of SCSe [31].

For those studies that focus on vapor-phase infrared signatures of such solids, the solid sample and gas cell are generally heated to higher temperatures to increase the analyte pressure. For instance, anthracene [32] was heated to 100 °C, phenanthrene [32] heated to 90 °C, 1-azaindolizine [33] and dimethylquinolines [34] heated to 80 °C. The objective of the present work is thus to develop a technique to determine quantitative 50 °C gas-phase IR spectra for those compounds that naturally exist as solids but have sufficient vapor pressures to be observed as gases in the atmosphere. We systematically develop such a method using the compounds listed in Table 1.

## 2. Experimental

### 2.1. Acquisition parameters for static system

The methodologies and instrumentation used to collect the vapor-phase data have been previously described [1,2,11,12,24]. The most important aspects of this method are: 1) the data are quantitative, with each composite spectrum derived from 10 or more individual measurements and 2) the spectral resolution is 0.11 $cm^{-1}$, corresponding to the most narrow pressure-broadened linewidths for measurements made at or near atmospheric pressure. The instruments are calibrated daily on both the wavelength and absorbance axes [3,35,36].

To compare results for the new solids flow-method data, a composite spectrum was also generated for camphor vapor using the passive vaporization method. Eight pressure-pathlength burdens were measured using a gold-plated 20 cm gas cell at 70 °C. Each camphor burden was first measured neat without $N_2$-ballast gas and subsequently adding UHP nitrogen to the sample for a total pressure of ca. 760 Torr. Camphor pressures (between 0.07106 and 0.30042 Torr) were measured using an MKS 690A 1-Torr precision Baratron and the total camphor/nitrogen pressures were measured using an MKS 690A 1000-Torr head. These spectra were recorded using a Bruker IFS 125 HR spectrometer with an instrumental resolution of 0.112 $cm^{-1}$, co-adding 256 scans in most cases. The camphor spectra all exhibited small amounts of $H_2O$ and $CO_2$ which were subtracted from the spectrum by using reference spectra of water and air taken on the same instrument.

### 2.2. Instrumental characteristics of flow system

Briefly, for the solids work, a Bruker IFS 66v/S vacuum spectrometer [37] was used with vacuum also maintained in the accessory chamber that houses the White cell. The cell interior was maintained at ambient pressure, typically between 748 and 766 Torr by a flow of dry nitrogen. Relevant parameters associated with data acquisition and processing

**Table 1**
Physical properties for the solvents and analytes used.

| Compound | Rm. Temp. Phase | Molecular Weight (g/mol) | Density ($g/cm^3$) @ 25 °C | Melting Point (°C) | Boiling Point (°C) | Vapor Press. (Torr) @ 25 °C |
|---|---|---|---|---|---|---|
| Carbon Disulfide | Liquid | 76.14 | 1.2557 | –112 | 46 | 360.78 |
| Carbon Tetrachloride | Liquid | 153.82 | 1.58402 | –23 | 77 | 99.8 |
| Camphor (racemic mix) | Solid | 152.23 | 0.992 | 179 | 204 | 0.65 |
| Dicyclopentadiene | Solid | 132.20 | 0.924 | 34 | 170 | 2.3 |
| Menthol | Solid | 156.27 | 0.89 | 47 | 215 | 0.10 |
| Naphthalene | Solid | 128.17 | 1.1412 | 80 | 218 | 0.083 |
| Phenol | Solid | 94.11 | 1.071 | 41 | 182 | 0.332 |
| Syringol | Solid | 154.16 | 1.134 | 57 | 261 | 0.01 |

*vapor pressures are from nwir.pnl.gov [2].

have been previously documented [1,2]. A glow bar source, a Ge-on-KBr beamsplitter, and a photoconductive mercury cadmium telluride (MCT) detector were used, in addition to a custom second aperture assembly. Since the solids can only achieve small gas-phase mixing ratios, a long-path cell (set to 8.05 m) increases the path length and the active disseminator is used to quantitatively generate the gas mixtures [22]. The optical system has been corrected for both the "warm aperture" [1] and double modulation [38] artifacts.

As previously described, the White cell flow system has a unique configuration whereby the cell experiences a flow of dry nitrogen gas from liquid $N_2$ boil off at all times; the continuous $N_2$ gas flow is regulated by an MKS model 1859A-050L-8 V mass flow controller; 25 standard liters per minute is the typical flow rate. The heated $N_2$ gas flows across a stainless steel T-piece heated to ca. 25 °C below the analyte's boiling point [22], the analyte injected from a syringe across a heated sloped surface. It is assumed that all liquids or solutions are vaporized and eluted by the carrier gas. To ensure complete mixing of the gases at all temperatures prior to entering the White cell, the mixture enters a Metra model 1060–002 L mixing chamber, demonstrated to provide thorough gas mixing. (increased Reynolds number). The mixture enters the White cell where it is interrogated by the IR beam in the thermostatted 6.0 L volume White cell. The gas is vented directly to the building exhaust and the cell is thus at ambient pressure at all times, near 760 Torr. Suspended into the White cell are both a thermocouple temperature gauge and a NIST-traceable pressure gauge. The exact pressure is monitored inside the cell for each measurement and recorded so as to calculate the total number density of analyte molecules in each burden that go into the composite measurement. All transfer lines are stainless-steel passivated (Sulfinert®, Restek Corp) ½-inch transfer lines maintained above room temperature along their entire length to prevent analyte condensation. The disseminator dispenses the liquid at a fixed volume rate from a syringe pump onto a heated stainless steel surface where it is vaporized into the $N_2$ gas flow. The liquid is pumped into the $N_2$ flow at different flow rates to generate a series of spectra, each with a unique partial pressure [22]. The averaging scheme uses a weighting mechanism that also corrects for photometric nonlinearity deviations. The absorbance is scaled using optical methods to confirm the path length using known absorbers, commonly isopropyl alcohol (IPA) [3]. Using ten or more burdens and the intensity weighting scheme, the data are reduced to produce a single composite (1 ppm-m at 296 K, 1 atm) spectrum [2].

### 2.3. Solution preparation

Solid analytes were purchased from Aldrich Chemical with the following purities: Menthol (99 %), dicyclopentadiene (99.4 %), syringol (99 %), naphthalene (99+%), phenol (99 %) and camphor (96.2 %). The solvents were of the highest obtainable purity: Reagent plus > 99.9 % carbon disulfide and 99+% carbon tetrachloride. All chemicals were used as supplied from the vendor. While solutes of the highest purities are used, it is not uncommon for a 1 or 2 % impurity in the solute to be present. This corresponds to ~1 or 2 % error in the resulting cross-sections. The results incorporate this error when there are known and quantified impurities which can be used to scale the final result. The impurities present and any scaling are all noted in the metadata for each molecule. In some cases, the certificate of analysis (COA) from the manufacturer provides information as to potential impurities and their fractions. Table 1 displays salient physical properties. Solutions were prepared both volumetrically and gravimetrically by weighing the empty volumetric flask with stopper, adding the solid to it, wiping the rim and re-weighing the flask and stopper plus solid. This avoids most errors associated with non-quantitative transfer. The solvent was added to the flask and the solute dissolved. Additional solvent was added to the volumetric line. The solution concentration was recorded gravimetrically; the total mass was obtained by re-weighing the flask with stopper, solute and solvent.

To describe the analytical procedure, menthol (CAS#89–78–1) is used as an example. A pre-test was first conducted to help establish a practical solubility limit; it was found that approximately 10 to 12 g of menthol would conveniently dissolve in 20 ml of $CCl_4$ while 14 to 16 g would dissolve in 20 ml of $CS_2$. Since a homogeneous solution without precipitate is required, menthol masses were selected significantly below these solubility limits. To obtain quantitative spectra for menthol, 5.445 ± 0.002 g (0.03484 mol) of the crystalline solid were dissolved in 22.034 ± 0.002 g (0.14325 mol) of $CCl_4$ in a 20 ml volumetric flask. The calculated concentrations in moles/μl were $1.742 \times 10^{-6}$ and $7.163 \times 10^{-6}$, for menthol and $CCl_4$, respectively. Since one of the greatest sources of error is in preparing the solutions, the entire process was repeated. For the second solution, 7.303 ± 0.002 g (0.04673 mol) of menthol was dissolved in 18.599 ± 0.002 g (0.12092 mol) of $CCl_4$. The molar concentrations in this case were $2.337 \times 10^{-6}$ and $6.046 \times 10^{-6}$ mol/μl for menthol and $CCl_4$, respectively. Finally, to accommodate for the fact that the solute may have an absorption feature at the wavelengths of the strong $CCl_4$ bands, two solutions of menthol in $CS_2$ were prepared in a similar manner. For these, the molar concentrations in mol/μl for menthol were $1.540 \times 10^{-6}$ and $2.158 \times 10^{-6}$. The $CS_2$ concentrations were $1.201 \times 10^{-5}$ and $1.029 \times 10^{-5}$ mol/μl for the two solutions.

Data were acquired using a Hamilton 500 μl gas-tight fixed syringe with the White cell thermostatted at 25 °C. A Harvard Apparatus PHD 2000 infusion pump delivered liquid into the $N_2$ flow stream at a controlled rate, typically measured in μl/min. Multiple burdens were collected by adjusting the syringe pump flow rate. The number of moles of solute and solvent dispensed per unit time ($R_{solute}$ and $R_{solvent}$, respectively) is found by multiplying the sample injection rate in μl/min by the concentration in moles/μl. These values, along with the molar rate of the carrier gas ($R_{N2}$ in moles/min) and the measured cell pressure ($P_{cell}$), yield the partial pressure of the sample ($P_{sample}$) as follows:

$$\text{Sample Partial Pressure}\left(P_{sample}, \text{Torr}\right) = \left(\frac{R_{solute}}{R_{N2} + R_{solvent} + R_{Solute}}\right) P_{cell}(\text{Torr}) \quad (1)$$

The gas-phase mixing ratio of the sample ($C_{sample}$ in ppm) can be obtained by dividing the partial pressure of the sample ($P_{sample}$) by the cell pressure ($P_{cell}$) and multiplying by $10^6$. We assume all gases are ideal.

$$C_{sample}\ (\text{ppm}) = \left(\frac{P_{sample}}{P_{cell}}\right) 10^6 \quad (2)$$

Once the sample pressure has been calculated, the data processing proceeds exactly as with gas or liquid measurements described in previous publications [2,22]. A plot of the absorbance (A using base 10 logarithms) vs. concentration (C) × pathlength (d) at each wavenumber bin yields the absorption coefficient ε(v, T) as slope via the Beer - Lambert law

$$A(v, T) = \varepsilon(v, T) dC \quad (3)$$

where for a "concentration" in Torr and a pathlength d in cm the absorption coefficient corresponds to a burden of 1 Torr-cm at the cell temperature. This is converted to the equivalent burden at 296 K by multiplying by the ratio of the actual temperature to 296 K. The absorbance in $(\text{ppm-m})^{-1}$ is then computed by converting cm to meters and Torr to ppm at atmospheric pressure.

## 3. Results and discussion

### 3.1. The infrared reference spectra of neat carbon disulfide and carbon tetrachloride

For these applications, both $CS_2$ and $CCl_4$ are desirable as solvents since they have a small number of strong IR absorption bands in the

wavenumber range of interest; each exhibit just one fundamental band in the important longwave infrared (LWIR) spectral domain. Consideration was also given to other infrared spectroscopically inert solvents. For example, deuterated chloroform or some perfluorinated or perbrominated species, preferably of high symmetry such as $CBr_4$, may be used, but for these experiments, we utilized only $CS_2$ and $CCl_4$. This study has focused on the $600 < \tilde{\nu} < 2000$ $cm^{-1}$ region and Fig. 1a displays the quantitative reference spectra of both $CS_2$ and $CCl_4$, from the PNNL gas phase database [2], each representing an optical depth of 1 ppm-m at 296 K; the spectra are offset for clarity. In Fig. 1a, the $\nu_3$ antisymmetric stretch fundamental band of carbon disulfide ($D_{\infty h}$ point group symmetry) appears at 1535 $cm^{-1}$ and the $\nu_3 + \nu_2 - \nu_2$ hot band, at 1529 $cm^{-1}$ is buried under the $\nu_3$ band. In Fig. 1b, the $^{13}CS_2$ $\nu_3$ band can be seen at 1485 $cm^{-1}$, and the $\nu_3 - \nu_1$ difference band[39] is at 878 $cm^{-1}$. For carbon tetrachloride ($T_d$ point group), the $\nu_3$ and $\nu_1 + \nu_4$ Fermi resonance dyad is observed at 790 $cm^{-1}$ in Fig. 1a. [40], and weaker combination bands are show in Fig. 1b [41].

Multiple flow rates of $CS_2$ and $CCl_4$ (separately) were used to measure the quantitative infrared spectra of these compounds. Once the composite spectrum was calculated, we used the solvent reference spectra to subtract the solvent spectral features.

### 3.2. Example analysis: dicyclopentadiene in $CS_2$ and $CCl_4$

In this work we report the disseminator-flow method results for six solid analytes: menthol, syringol, dicyclopentadiene, camphor, naphthalene and phenol. All species were run in both $CCl_4$ and $CS_2$ except for naphthalene, which was analyzed only in $CS_2$. As an example, the analyte dicyclopentadiene is used to demonstrate how to identify analyte features and develop the composite spectrum. Fig. 2a displays the curve of growth for 4 of the 15 dicyclopentadiene burdens run in $CS_2$ (8.45 mol % dicyclopentadiene, 91.55 mol% $CS_2$), all at 25 °C. The data correspond to burdens of 12.0, 21.0, 35.0 and 51.0 μl/min liquid solution disseminated into 21.16 standard liters per minute (SLPM) nitrogen carrier gas, corresponding to gas-phase mixing ratios for dicyclopentadiene of 16.1, 28.2, 47.0 and 68.4 ppm (μmol/mol), respectively. It is seen that the $\nu_3$ fundamental $CS_2$ band at 1535.32 $cm^{-1}$ is completely saturated, obfuscating any dicyclopentadiene signal in that region: There is in fact a dicyclopentadiene band obscured by the $\nu_3$ mode for $CS_2$, so $CCl_4$ was used as a second solvent. Fig. 2b displays the dicyclopentadiene growth curve for a solution of 11.3 mol% dicyclopentadiene in $CCl_4$ at 25 °C. The four plotted dissemination rates (of 16 total) are for 10.0, 17.0, 31.0 and 42.0 μl/min, corresponding to gas-phase mixing ratios for dicyclopentadiene of 11.9, 20.2, 36.8 and 49.8 ppm (μmol/mol). The strong $CCl_4$ $\nu_3/\nu_1 + \nu_4$ bands and weaker combination band are seen in Fig. 1b, but at different frequencies than the $CS_2$ bands, allowing the $CS_2$-obscured dicyclopentadiene bands to be revealed.

Composite spectra for dicyclopentadiene dissolved in $CS_2$ and $CCl_4$ were developed using 15 burdens of dicyclopentadiene in $CS_2$ and 16 burdens of dicyclopentadiene in $CCl_4$. To account for nonlinearities, each burden is weighted at each wavenumber bin $\tilde{\nu}$ by a factor of $T^2(\tilde{\nu})$ (where $A = -\log_{10} T$), and data with $T \leq 0.025$ are simply weighted with zero [22]. The composite spectra are normalized to a 1 ppm-meter burden at 296 K of the analyte but still contain noticeable solvent bands. The $CS_2$ and $CCl_4$ combination, overtone and isotopologue bands (Fig. 1) are subtracted from each composite spectrum, whereas spectral domains of $CS_2/CCl_4$ saturated fundamentals are simply removed; a final continuous composite spectrum is created by averaging the result in regions where neither solvent interferes but using one or the other result as appropriate in regions of solvent interference. To obtain a complete analyte spectrum in this manner, it is important that solvent bands do not overlap with each other. Fig. 2c displays the final dicyclopentadiene composite spectrum in the 600 to 1700 $cm^{-1}$ range corresponding to 1 ppm-meter at 296 K.

### 3.3. Precision and uncertainty analysis

In a previous disseminator study using only neat liquid analytes, the systematic (Type A) [2,22,42] uncertainty was estimated to be 7 %. This

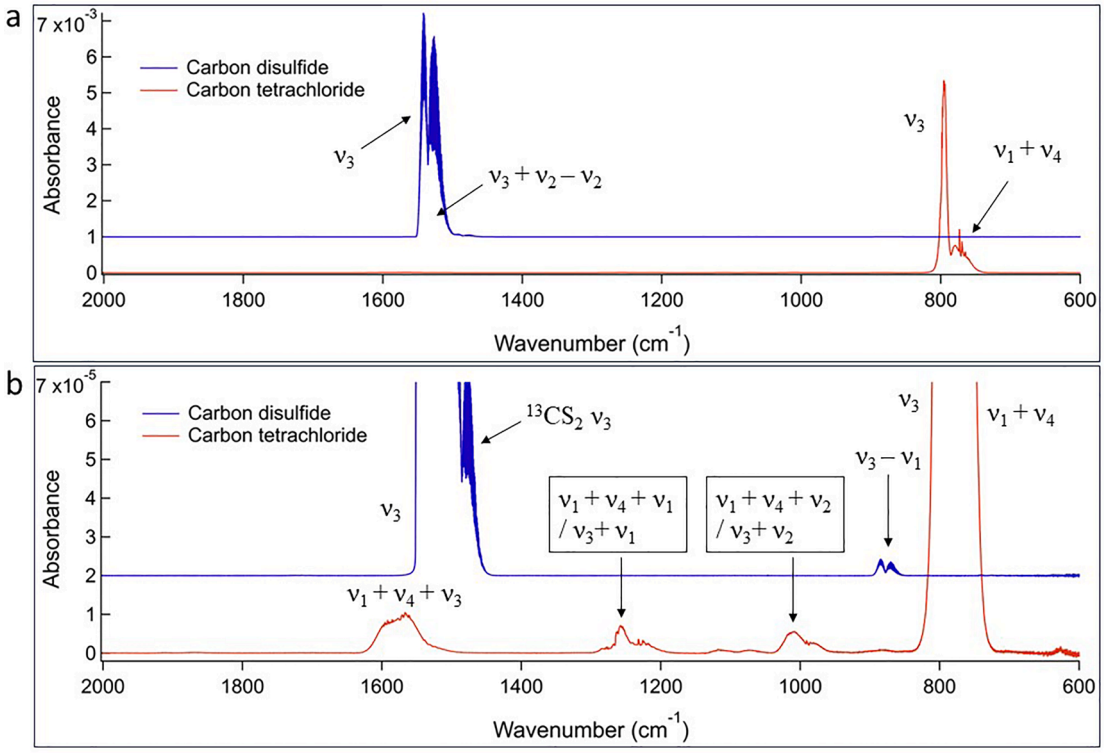


**Fig. 1.** Vapor-phase spectra of the two solvents $CS_2$ and $CCl_4$: a) Composite spectra for $CS_2$ and $CCl_4$ where the ordinate is in units of $(\text{ppm-meter})^{-1}$ optical burden at 296 K. b) Same spectra but with the y-axis expanded by a factor of 100. The $CS_2$ spectrum, in blue, has been offset for clarity.

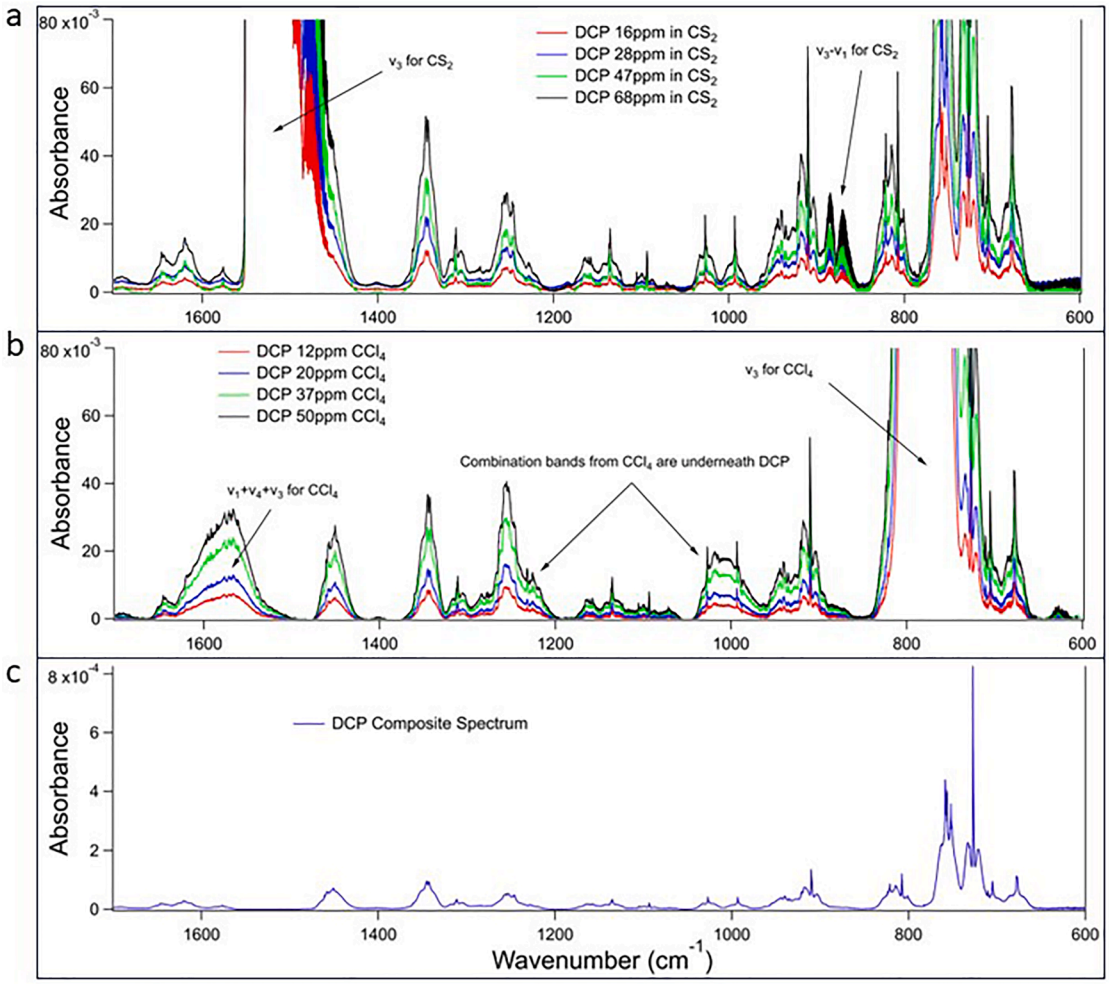


**Fig. 2.** Example 25 °C curve of growth for dicyclopentadiene (DCP) dissolved in a) $CS_2$ and b) $CCl_4$ with only 4 burdens displayed in each for clarity. c) Composite spectrum derived from 15 $CS_2$ and 16 $CCl_4$ burdens; the $CS_2$ and $CCl_4$ bands removed via subtraction and the composite spectrum corrected by rescaling.

value characterizes systematic uncertainties at a 2σ confidence level and was derived using equation 5 and the fractional values in Table I of reference 22. In such analyses, the calculation of absorbance begins with the Beer-Lambert law, Eq. (3). To estimate the uncertainty in the absorption coefficient ε, we add in quadrature the estimated uncertainties in A (absorbance), C (concentration) and d (path length). From the ideal gas law, the calculation of C includes a measurement of both pressure (P) and temperature (T). The concentration, C, of the solute in the cell is determined by its mole fraction in the overall gas flow and the cell pressure. Because the solutions are made up gravimetrically and volumetrically, the molar density of the solute and solvent are found by dividing the moles of each by the final volume.

$$Moles(solute) = \frac{Mass\ (with\ solute) - Mass\ (Empty\ Flask)}{Molecular\ weight\ (solute)} \quad (4)$$

A similar approach is used to calculate the moles of solvent. For each weighing, the masses are measured to ±0.001 g, with the solvent masses in the 25 to 40 g range, while the solute is typically 1 to 8 g. The molar volume uncertainty is typically dominated by the uncertainty of the volume measurement, taken to be ~0.1 % for a 20 ml volumetric flask. Multiplying the molar density (in mol/μl) by the infusion rate (in μl/min) yields the molar flow rate of each. The infusion rate is estimated to be accurate to ±1 %. This is an order of magnitude greater than the uncertainty in molar volume, so the solute and solvent molar flow rate uncertainties are taken to be ~1 %. The molar flow rate of nitrogen ($R_{N2}$) is estimated from the manufacturers specifications to be accurate to ±2 %. The solute gas-phase partial pressure ($P_{solute}$) in the gas cell is thus given by Eq. (1) where $R_{N2}$ is greater than that of the other two factors in the denominator. The overall uncertainty in the cell pressure ($P_{cell}$) is thus estimated (see [ref. 22]) to be 1 %. The uncertainty in the solute concentration is calculated by adding the uncertainties in quadrature, namely $\Delta C = (0.01^2+0.02^2+0.01^2+0.01^2)^{1/2}$ ~2.6 %. The exact pathlength, d, of the White cell is difficult to measure but the uncertainty is estimated to be ~2 %. The absorbance (A) uncertainty[22] is a result of instrument drift (0.002) and detector non-linearity (0.02), or ~2 %. The final normalization of ε to 296 K requires multiplying by $T_{cell}$ (296) where the uncertainty in T is ~1 %. These results are summarized in Table 2. The square root of the sum of the squares thus suggests a 2σ uncertainty of 8 %. As might be expected, due to the added chemical dissolution step, the composite uncertainty value is just slightly greater than that of the liquid's disseminator value alone (7 %).

**Table 2**
Maximum estimated systematic uncertainties associated with optical measurements/solution preparation.

| Symbol | Value (fraction) | Uncertainty Major Source |
|---|---|---|
| ΔA (estimated) | 0.02 | Detector (HgCdTe) non-linearity |
| ΔC (estimated) | 0.026 | Pressure of gas in White cell |
| Δd (estimated) | 0.02 | Uncertainty in optical path |
| ΔT (estimated) | 0.01 | Drift, thermal equilibration rates |
| 2σ estimate of uncertainty | 0.08 | |

### 3.4. Analytical reproducibility

To investigate the analytical reproducibility including effects of solution preparation, a series of example measurements was carried out using menthol as the analyte. Four solutions were prepared, two each in $CS_2$ and $CCl_4$. The objective was to construct a composite spectrum for each solution, and compare the analytical reproducibility spectra via the use of band integration [43]. In each case a composite spectrum normalized to 1 ppm-meter at 296 K was calculated. Table 3 summarizes the calculated molar densities for each solution. Combining these values with the injection rate in ml/min yields a direct calculation of the mole fraction of solute in the gas flow as long as the diluent molar flow rate is also known.

Figs. 3a and 3b display the menthol spectra before and after $CCl_4$ and $CS_2$ subtraction, respectively. Before solvent subtraction, the $\nu_3$ fundamental band for $CCl_4$ is clearly present and some of the combination bands overlap features associated with the menthol spectrum. As for the $CS_2$ solution in Fig. 3b, the $CS_2$ $\nu_3$ fundamental band dominates the spectrum while the combination band for $CS_2$ forms a shoulder on a weak menthol feature. The inset shows an isolated band in $CS_2$ compared to the measured spectrum of menthol after scaling the $CS_2$ to the calculated molar ratio of solvent to solute. To gauge both the reproducibility of preparation as well as using different solvents, the area between the $CCl_4/CS_2$ $\nu_3$ fundamental bands (1425 – 832 $cm^{-1}$) were calculated. Table 4 contains the spectral integration results for all four menthol solutions (spectra shown in Fig. 4) after solvent subtraction. The agreement is reasonable, given the error sources mentioned above. It should be noted that menthol was a somewhat problematic solute due to its tendency to deposit on system surfaces.

As a second test of the technique at 50 °C, syringol was dissolved in a similar manner in $CS_2$ and $CCl_4$ separately, two solutions each. The makeup of the solutions is given in Table 5. After baseline correction and removal of the large solvent bands, the resulting four syringol spectra are shown in Fig. 5, with band integrals found in Table 6. For syringol, the percent standard deviation ranged from 3.3 to 5.5 % which is consistent with the 8 % estimate for the uncertainty. The general shape of the spectrum is reliably extracted from both solvents, but the quantitative reproducibility is limited by the experimental factors.

### 3.5. Results for six solid molecules using solution disseminator-flow method

We note that three of the solid species analyzed in this paper, in fact had their quantitative data made available in previous public releases; these include naphthalene [2], as well as phenol and syringol [12]. Both 2- and 3-methoxyphenol spectra were also previously released, but these are liquids which were measured on the disseminator system. We also note that the alcohols syringol and menthol were the most challenging in both the laboratory and data reduction due to their lower vapor pressures (Table 1) and "sticky" chemical nature.

Fig. 6 presents the results for the six title molecules of this study; each spectrum is a composite derived from a dozen or more measurements in solvents $CS_2$ and $CCl_4$, except naphthalene which was measured only in $CS_2$. Of these, camphor is an optically active molecule and its infrared [28,44–46] and Raman [47] vibrational circular dichroism (VCD) spectra have been exhaustively measured in the solution phase. The molecule's modest size makes it a convenient VCD model system and computational results for molecular structure, vibrational frequencies, dipole and VCD rotational strengths have been compared to experimental results [28,44–46]. It has also been studied for parity violation effects [48,49]. Despite extensive spectroscopic literature generated regarding this molecule, there appears to be no peer-reviewed quantitative IR absorption cross section measurement for the vapor phase of camphor.

Cyclopentadiene is part of the C5 stream in petroleum and coal tar refining and it is separated from other components in the C5 stream by first forming its higher boiling point dimer, (endo)-dicyclopentadiene. The monomer is then regenerated via heating [50,51]. The kinetics of cyclopentadiene dimerization and the reactions of cyclopentadiene with other C5 compounds (isoprene, for example) have been studied extensively [52,53]. While the vapor-phase infrared spectrum of cyclopentadiene has been assigned [54], to our knowledge no quantitative infrared spectra of this compound have been reported in the literature. For dicyclopentadiene, its complete vapor-phase vibrational spectrum has yet to be assigned, though Tjahjono et al. [55] have measured quantitative infrared spectra of cyclopentadiene and dicyclopentadiene dissolved in toluene, and Schaubroeck et al. [56] report a partially assigned solution phase Raman spectrum.

The vibrational assignments for syringol [57], menthol [59,60], phenol [58,59], and naphthalene [60] have also been previously reported for these species, mostly in the condensed phase. It appears, however, the only quantitative gas-phase spectra are to be found in the HITRAN database [61] and those are from PNNL measurements. Further vibrational assignments of the six species, e.g. using band structure [62], will not be pursued here as it is beyond the scope of the present paper. It is emphasized, however, that the spectra seen in the Fig. 6 are some of the very few quantitative gas-phase infrared spectra of species that naturally occur as solids at room temperature. In the plot, the y-axis is quantitative and has a scale of $(ppm\text{-}meter)^{-1}$, where each spectrum in the plot has successively been offset by 0.001 on the y-axis for clarity. It is seen that for all six spectra, the stronger bands have maximal peak heights on the order of 1 to $2 \times 10^{-3}$ $(ppm\ meters)^{-1}$, with the maximal values for the planar aromatics (phenol, naphthalene, dicyclopentadiene) found in the narrow Q-branches of the in-phase symmetric ring C—H bending modes [6] between 740 and 795 $cm^{-1}$. As such, all six are some of the stronger IR-absorbers of the ~600 molecules in the PNNL database [3]. The importance of recording data at (medium-) high resolution [63] is also observed in the figure; some of these pressure-broadened spectra manifest very narrow Q-branch peaks, several with FHWM (Full Width at Half Maximum) $\leq$ 1.0 $cm^{-1}$. For example, the phenol Q-branch at 782 $cm^{-1}$ has $\Delta\tilde{\nu} = 0.7$ $cm^{-1}$, with individual Q-branch lines (0–0, 1–1, etc.) of $\Delta\tilde{\nu} \sim 0.1$ $cm^{-1}$. Such peak(s) clearly lend themselves to standoff gas-phase detection via e.g. QCL laser spectroscopy [64].

**Table 3**
Menthol solution calculations.

| | In $CCl_4$ | | In $CS_2$ | |
|---|---|---|---|---|
| | Solution 1 | Solution 2 | Solution 3 | Solution 4 |
| Empty Flask (g) | 58.871 | 59.035 | 59.048 | 58.592 |
| w/Menthol (g) | 64.316 | 66.338 | 65.793 | 63.405 |
| w/Menthol + solvent (g) | 86.35 | 84.937 | 81.456 | 81.694 |
| Volume (ml) | 20.0 | 20.0 | 20.0 | 20.0 |
| Menthol (g) | 5.445 | 7.303 | 6.745 | 4.813 |
| Solvent (g) | 22.034 | 18.599 | 15.663 | 18.289 |
| Menthol (mol/μl) | 1.74E-06 | 2.34E-06 | 2.16E-06 | 1.54E-06 |
| Solvent (mol/μl) | 7.16E-06 | 6.05E-06 | 1.03E-05 | 1.20E-05 |

### 3.6. Accuracy analysis

To estimate an absolute accuracy for the new technique, three different methods were used to assess the absorption cross sections: 1) performing the same gravimetric analysis but instead of a solid analyte, dissolving a liquid analyte whose cross sections are known (isopropyl alcohol), 2) making a comparison between a composite spectrum from the flow system to that for the passive vaporization system using one of the species (camphor), and 3) comparing literature values to what other researchers have found when assessing some of the same species as in this study.

#### 3.6.1. Isopropyl alcohol dilution comparison

Two solutions of IPA in $CCl_4$ were prepared gravimetrically and

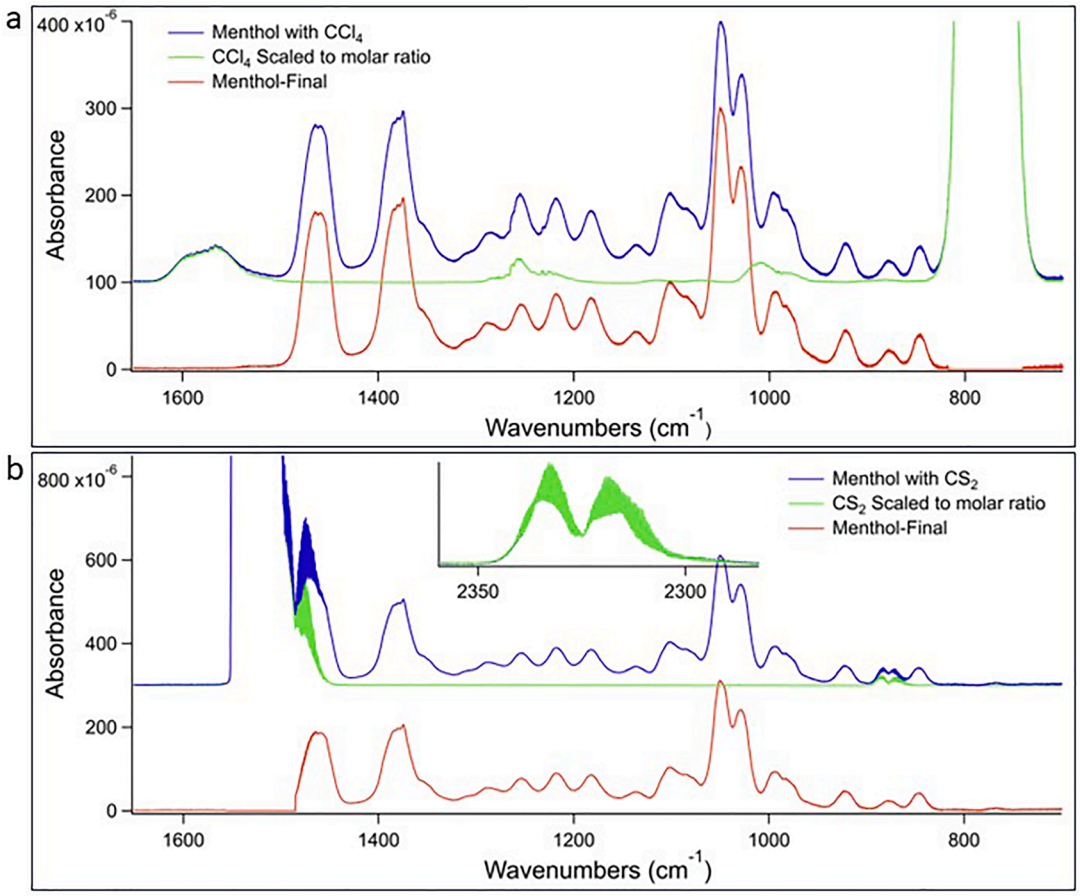


**Fig. 3.** Vapor-phase spectra of menthol a) dissolved in $CCl_4$ and b) $CS_2$ at 50 °C. The spectra before solvent subtraction along with the scaled solvent reference spectrum are offset for clarity. The lower plot inset contains menthol in $CS_2$ and the $CS_2$ reference spectrum scaled by the molar ratio of solvent to solute.

**Table 4**
Infrared band integrals for four separate preparations of menthol in $CCl_4$ and $CS_2$ shown in Fig. 4.

| | Region 1<br>1425–1325 $cm^{-1}$ | Region 2<br>1122–943 $cm^{-1}$ |
|---|---|---|
| Solution 1 - $CCl_4$ | 0.00826 | 0.0182 |
| Solution 2 - $CCl_4$ | 0.008659 | 0.0190 |
| Solution 3 - $CS_2$ | 0.009067 | 0.0201 |
| Solution 4 - $CS_2$ | 0.00858 | 0.0187 |
| Average | 0.0087 ± 0.0003 | 0.019 ± 0008 |
| std Dev. (%) | 3.8 | 4.2 |

volumetrically in a manner similar to that for the solids as described above. The resulting molar densities were calculated, and an IPA spectrum computed. Fig. 7 shows the comparison of the two solutions measured at 50 °C utilizing 10 burdens in each case. Included in the figure is the 50 °C result from the NWIR (Northwest Infrared) database. Integration of several regions show the error bars are within expected values. Note that the IPA signal is relatively small due to the dilution with $CCl_4$. This low concentration decreases the resulting signal-to-noise in the red and blue traces, but the agreement with the passive vaporization data is a good indicator of high accuracy.

Table 7 contains the associated results of integrating the noted bands in the IPA spectra. The average of two measurements nicely matches the database values, as expected from the results of Fig. 7.

### 3.6.2. *Static vs. flow comparison*

We also compare the disseminator-flow method analysis to the passive vaporization method (as was used for hundreds of molecules in the NWIR data set) using camphor as a test case. Camphor is a waxy solid at room temperature with a vapor pressure of only ca. 0.4 Torr at 70 °C. In practice, actual passive vaporization measurements are made only to maximal pressures of perhaps 50 % of the analyte's vapor pressure to avoid condensation on any "cold spots". These physical constraints make camphor a very challenging material for static measurements, but a good candidate for the solution method discussed here. Figs. 8a-b display the composite spectra for gaseous camphor generated using the passive and flow methods (after solvent-band subtraction). The passive spectrum represents eight individual burdens at 70 °C ranging from 0.07 to 0.3 Torr. The flow system-derived spectrum represents 13 to 14 burdens ranging from 0.002 to 0.12 Torr of camphor in $CS_2$ or $CCl_4$. Qualitatively, the spectra look very similar, and integrated areas agree to within ~6 %, but the static cell absorbance values are systematically less than the flow system data. This could be a result of unavoidable condensation in the static system at higher pressures. However, the use of a White cell clearly allows for much lower pressure measurements while delivering excellent signal-to-noise ratios. Fig. 8a illustrates the improvement in signal-to-noise obtained with the longer path. Despite the lower signal level seen for the static method, the band integrals agree to ca. 6 %, again within the 8 % estimated systematic uncertainty.

### 3.6.3. *Literature comparison*

A final method to assess the accuracy of IR cross-sections is to compare results to those of other researchers. There have been studies of three compounds (two liquids, one solid) whose data were obtained by other groups and then compared to PNNL data that had been derived using the present methods and where the data had been previously released by PNNL [12]. This includes syringol whose spectrum is discussed below. Four of the PNNL composite spectra reported here

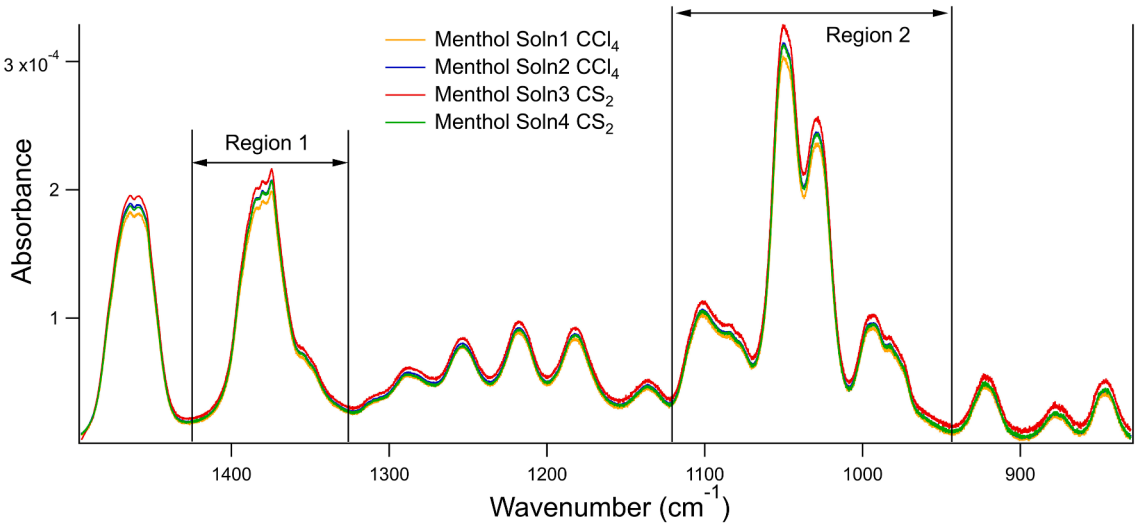


**Fig. 4.** Four separate measurements of menthol in two solvents. Spectra temperature are 50 °C. The band integrals are given in Table 4.

**Table 5**
Chemical composition by mass and volume for four syringol solutions in $CCl_4$ and $CS_2$.

| | In $CCl_4$ | | In $CS_2$ | |
|---|---|---|---|---|
| | Soln 1 | Soln 2 | Soln 3 | Soln 4 |
| Empty Flask (g) | 58.613 | 58.889 | 58.613 | 59.074 |
| w/Syringol (g) | 60.076 | 60.622 | 59.893 | 60.661 |
| w/Syringol + solvent (g) | 89.567 | 89.838 | 83.503 | 83.895 |
| Volume (ml) | 20 | 20 | 20 | 20 |
| Syringol (g) | 1.463 | 1.733 | 1.28 | 1.587 |
| Solvent (g) | 29.491 | 29.216 | 23.61 | 23.234 |
| Syringol (mol/μl) | 4.75E-07 | 5.62E-07 | 4.15E-07 | 5.15E-07 |
| Solvent (mol/μl) | 9.59E-06 | 9.50E-06 | 1.55E-05 | 1.53E-05 |
| Ratio (Solvent/Syringol) | 20.204 | 16.897 | 37.346 | 29.642 |

(naphthalene, phenol, syringol and menthol) are already found in the HITRAN infrared absorption cross-sections spectral library [61]. The composite spectra of dicyclopentadiene and camphor will be added to that library in the future and are also to be found in the supporting information of this paper. While several papers exist on condensed phase spectra of the six title compounds, review of the literature has, unfortunately, not revealed any quantitative gas-phase spectra for dicyclopentadiene, camphor or menthol to which the present results can be compared. For dicyclopentadiene, however, the gas-phase spectrum was at least compared to the liquid phase spectrum [65] to ensure that dissolving the compound in $CCl_4$ or $CS_2$ did not convert it back to cyclopentadiene. The composite flow system spectrum of dicyclopentadiene was compared to the liquid phase spectra of cyclopentadiene and dicyclopentadiene from the NIST Web Book, as well, and this comparison showed that the dicyclopentadiene does not convert to cyclopentadiene when dissolved in either $CCl_4$ or $CS_2$.

Cuisset et al. have reported vapor-phase infrared cross-sections for a series of methoxyphenol compounds including 2-methoxy, 3-methoxy and 2,6-dimethoxyphenol (syringol), the latter solid reported here. Using a synchrotron source for the far-infrared and a commercial FTIR spectrometer for the mid-infrared measurements, Cuisset and coworkers completed a thorough spectroscopic analysis, deriving quantitative IR cross-sections for these compounds, as well as two nitroguiacols [57]. They also compare their results to those three molecules whose IR cross sections had already been published by PNNL including

**Table 6**
Infrared band integrals for four separate preparations of syringol in $CCl_4$ and $CS_2$.

| Spectral Range ($cm^{-1}$) | 1410–992 | 1663–1566 | 3610–3550 | 3036–2798 |
|---|---|---|---|---|
| Solution 1 - $CCl_4$ | 0.1299 | 0.0155 | 0.0128 | 0.0336 |
| Solution 2 - $CCl_4$ | 0.1199 | 0.0140 | 0.0118 | 0.0300 |
| Solution 3 - $CS_2$ | 0.1252 | 0.0143 | 0.0125 | 0.0312 |
| Solution 4 - $CS_2$ | 0.1242 | 0.0136 | 0.0121 | 0.0321 |
| Average | 0.1299 | 0.0155 | 0.0128 | 0.0336 |
| % Std. deviation | 3.3 | 5.5 | 3.6 | 4.6 |

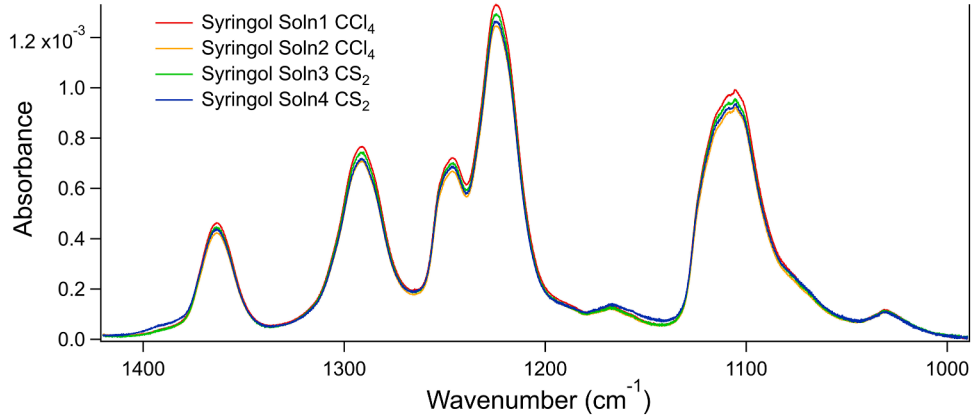


**Fig. 5.** Four separate measurements of syringol in two solvents. Spectra temperature are 50 °C. Band integrals are given in Table 6.

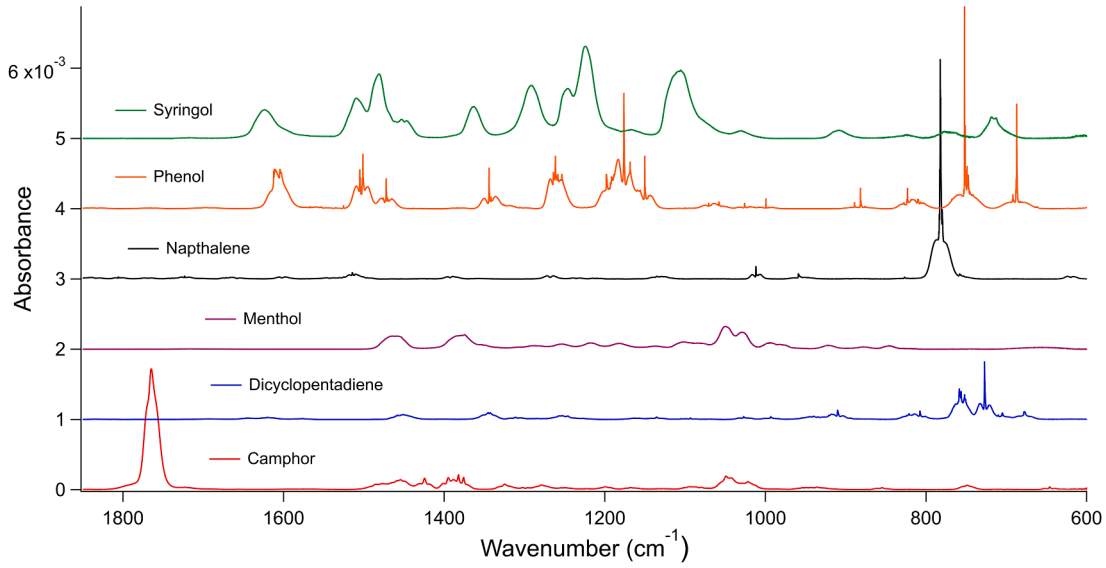


**Fig. 6.** Resultant composite spectra (50 °C) in the longwave infrared for camphor, dicyclopentadiene, menthol, naphthalene, phenol and syringol. Except for naphthalene, each is derived from multiple burden measurements (e.g. 15) for solutions in both $CS_2$ and $CCl_4$, the $CS_2$ and $CCl_4$ signatures removed via spectral subtraction and the composite spectrum corrected by rescaling. All spectra are quantitative with an optical depth of 1.0 ppm-m. Each spectrum in the plot has successively had 0.001 offset added for clarity.

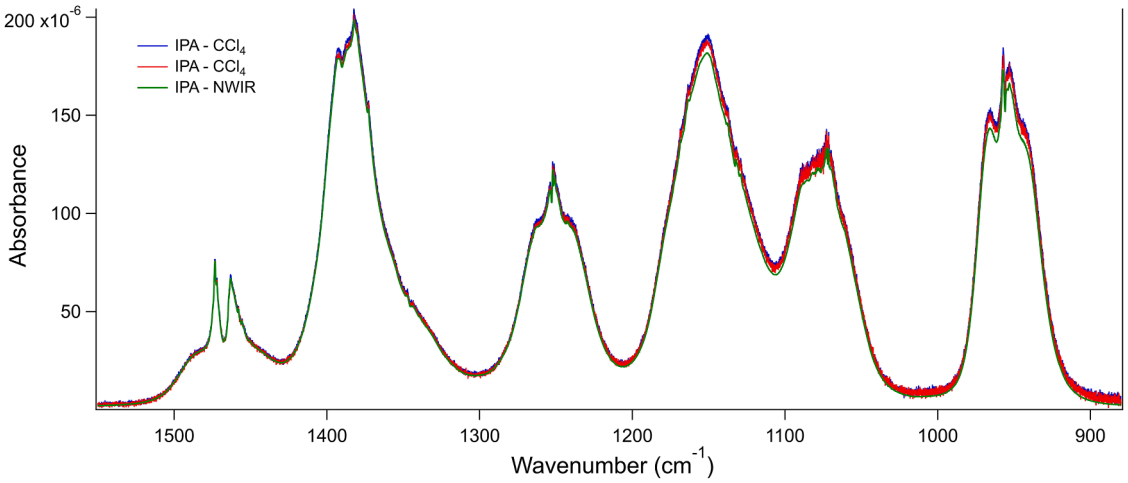


**Fig. 7.** Composite spectrum for isopropyl alcohol using the passive vaporization of neat liquid method (green dotted), as well as the flow system method where IPA was dissolved in $CCl_4$ at high (red) and low (blue) concentrations.

**Table 7**
Infrared band integrals for two separate preparations of IPA in $CCl_4$.

| Spectral range ($cm^{-1}$) | 1540–1010 | 3029–2703 | 3698–3600 |
|---|---|---|---|
| Solution 1-$CCl_4$ | 0.03642 | 0.03080 | 0.00241 |
| Solution 2-$CCl_4$ | 0.03585 | 0.03073 | 0.00242 |
| Average | 0.0361 | 0.0308 | 0.0024 |
| IPA-database | 0.0350 | 0.0310 | 0.0025 |
| % Difference | 3.4 % | 0.8 % | 2.4 % |

2-methoxyphenol, 3-methoxyphenol, and 2,6-dimethoxyphenol (2-MP, 3-MP and 2,6-DMP, respectively). In that comparison, Cuisset and co-workers divided the spectral analysis by using band integrals from 1000 to 1700 $cm^{-1}$ as well as from 2700 to 3700 $cm^{-1}$. The accuracy of those measurements, generated using passive vaporization, agreed very well with the PNNL data, on the order of 5 % for 2-MP, with agreement to ca. 10 % for the less volatile compounds, 3-MP and 2,6-DMP.

Naphthalene is of current interest not only as a pollutant and gas observed in biomass burning, but also because such PAHs (Polycyclic aromatic hydrocarbons) are thought to be the source of infrared emission bands in interstellar space. A partial report of the cross sections of naphthalene has been provided by Brackmann et al., who used an FTIR to measure a heated flow of gases from burning wood [66]. The spectra were calibrated using a weighed amount of each tar gas as it was observed running through a flow system. Cross sections were reported in Naperian units ($cm^2$/molecule) with a reported band integral area for only the 3020 to 3100 $cm^{-1}$ range. Their naphthalene integrated band area in this range is $0.8 \times 10^{-17}$ cm/molecule. After converting the present data to those units an integrated band area value of $1.51 \times 10^{-17}$ cm/molecule is obtained, meaning the Brackman et al. integrated area is 47 % smaller than the present results. While this is modestly good agreement, the lack of agreement may be related to their observation of condensation of the naphthalene on the KBr windows (and other cold spots) even though their flow system was heated to 400 °C. They compared their data for naphthalene to a polyaromatic hydrocarbon infrared spectral database from NASA-Ames, but whose experimental

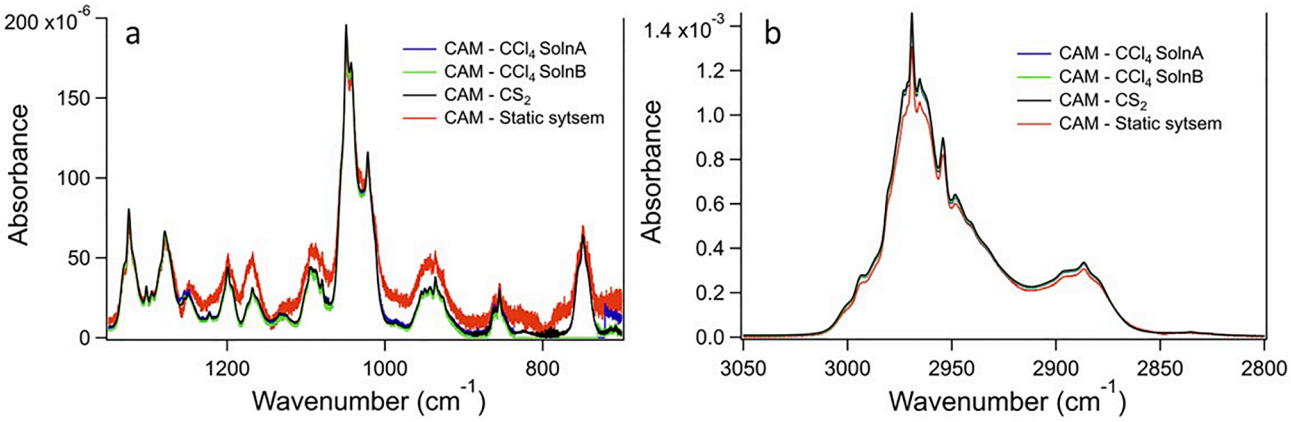


**Fig. 8.** Composite spectrum for vapor-phase camphor generated from both passive and flow systems. The ordinate is quantitative corresponding to 1 ppm-meter optical burden at 25 °C.

data are believed to represent cryogenic matrix isolation spectra. Brackmann et al. report that the 3020 to 3100$^{-1}$ integrated area for the NASA data is 1.2 × 10$^{-17}$ cm/molecule.

Phenol is one of the few solid-phase chemicals whose vapor-phase quantitative spectra have been reported. Etzkorn et al. report gas-phase infrared cross sections and integrated band areas for several aromatic compounds in both the infrared and ultraviolet, including phenol [67]. Those studies used an FTIR coupled to a White cell to make the IR measurements. Some of the solid or liquid target aromatic compounds were mixed with dichloromethane, the mixture simply injected with a syringe into a very large quartz White cell at room temperature; $N_2$ ballast gas was flowed over the syringe tip with a fan to mix the vapors. To facilitate comparison, the PNNL 25 °C phenol data were converted to Naperian cross section units (cm$^2$/molecule) and the spectra integrated over those wavenumber ranges of the Etzkorn paper. The results are presented in Table 8.

The present results and those of Etzkorn et al. agree reasonably well as seen in Table 8. There appears to be a systematic difference in the results whereby the Etzkorn et al. integrated areas are ca. 20 % lower than the PNNL cross-section values. Etzkorn et al. estimate the uncertainties for their phenol band areas to be at about ±3.5 %. This estimate comes from a combination of random and systematic uncertainties and appears to be a 1σ uncertainty. The PNNL band area uncertainties are given, as derived in Section 3.3, as ± 8 % (2σ). There are three technical advances of the last 25 years that would yield a better agreement for those results when comparing the two studies. These include: 1) the use of a thermostatted long path White cell which has gold coated surfaces to prevent adhesion. We suggest one possible shortcoming of the earlier experiment was the use of a quartz cell (needed for the photolysis experiments) which is not well suited for measurement of hydroxylated species such as phenols. 2) A second technological advance that may yield different results is the use of an improved disseminator system, whereby increasing the probability of complete volatilization of the sample. As originally reported by Nelson and coworkers [19,20,22,68], the disseminator method used for the current studies flash-volatilizes the sample. Finally, 3) for photometric accuracy, likely the most important advancement lies with the instrumentation whereby the nonlinear response from MCT detectors is corrected, either in the hardware using a preamplifier that is programmed to compensate for the non-linearity, or a software *ex post facto* correction for the MCT nonlinear response, as used in the present study [69].

**Table 8**
Comparison of band integrals for phenol over specific wavenumber domains.

| Spectral range (cm$^{-1}$) | PNNL integrated area (cm/molecule × 10$^{-18}$) | Etzkorn et al. area (cm/molecule × 10$^{-18}$) |
|---|---|---|
| 3626–3708 | 7.67 ± 0.61 | 6.36 ± 0.22 |
| 1577–1638 | 11.08 ± 0.89 | 8.26 ± 0.29 |
| 1231–1286 | 10.54 ± 0.84 | 8.26 ± 0.29 |
| 1121–1228 | 23.20 ± 1.86 | 18.50 ± 0.7 |
| 717–787 | 8.53 ± 0.68 | 6.45 ± 0.23 |

## 4. Summary

There now exist several spectral IR databases [70,71] that provide data for the many gas-phase species that can affect human health, threaten civil defense, warm the climate or pollute the air [61,72–76]. PNNL has recently developed two unique data sets that contain gas phase molecules emitted from biomass burning [12], as well as perfluoroalkyl substances (PFAS), which are currently of great environmental interest [3]. The motivation for this development stemmed from the potential use of open-path FTIR [77–79], infrared laser as well as (airborne) *in situ* measurements [78,79] for field monitoring emissions from e.g. biomass burning or PFAS contamination. For the optical methods, there is generally a dearth of quantitative IR reference spectra. During the course of generating such data sets, it became apparent that several of the compounds of interest were in fact semivolatile solids at room temperature. This includes single–ring and light polycyclic aromatic compounds (e.g. naphthalene, anthracene) [79], oxygenated aromatic compounds (phenol, syringol) [80], N-heterocyclic alkaloids [81] and mono- and di-carboxylic acids [82–84], all of which have been linked to biomass burning events. Camphor is of interest because it is a model chiral system [85] with well-studied VCD spectra; and dicyclopentadiene is of interest because of its dimerization kinetics of cyclopentadiene and its importance in petroleum refining [52].

Motivated by the above considerations, this work reports a novel method for measuring quantitative gas-phase spectra for such compounds which are solids at room temperature. Thus far, six compounds (dicyclopentadiene, phenol, menthol, syringol, naphthalene, camphor) have been studied using this approach; the technique appears widely applicable and reproducible. The quantitative spectra for camphor were obtained using both the flow and static systems, and the spectra generated via the flow system are effectively identical to the spectra generated with a static passive vaporization system. The static system is ideal for gases and high vapor pressure liquids, though it may be used for solids, but is limited to species with vapor pressures ≥ ca. 1 Torr. For either solid or liquid species with room-temperature vapor pressures lower than this value, passive vaporization measurements have proven frustratingly difficult: Any cold spots in the gas system cause condensation on the inner surfaces, requiring long (re-)equilibration times. The development of this flow system for the measurement of solid compounds in which (million-fold) dilution in $N_2$ gas lowers the analyte's partial pressure orders of magnitude less than its natural vapor pressure,

has proven useful at helping bypass the challenges associated with high temperature measurements. This is important because when quantifying gases in an infrared spectrum, the temperature of the reference spectra must be similar to the measured spectrum to ensure the best fit possible, especially if there are significant levels of interfering compounds, and the mixing ratio of the species of interest is in the low ppm range or lower. While a solid or a liquid of just 0.01 Torr vapor pressure may be considered relatively non-volatile, such a vapor pressure corresponds to an atmospheric mixing ratio of 13.2 $ppm_v$ (13,200 $ppb_v$), a quantity that can be of great environmental importance depending on the nature of the chemical. For such reasons, PNNL continues to expand its database with high resolution, high accuracy broadband infrared spectra with many compounds collected at three different temperatures: 5, 25 and 50 °C. The methods outlined in this study have been used to successfully create reference spectra for several solids of interest whose quantitative vapor-phase spectra have been seldom or never reported.

## CRediT authorship contribution statement

**Matthew D.W. Schneider:** Writing – review & editing, Methodology, Investigation, Formal analysis. **Tracy J. Baker:** Writing – review & editing, Writing – original draft, Visualization, Methodology, Formal analysis, Data curation, Conceptualization. **Nicole K. Scharko:** Writing – review & editing, Formal analysis, Data curation. **Thomas A. Blake:** Writing – review & editing, Writing – original draft, Validation, Methodology, Investigation, Formal analysis, Data curation, Conceptualization. **Russell G. Tonkyn:** Writing – review & editing, Writing – original draft, Visualization, Validation, Methodology, Investigation, Formal analysis, Data curation, Conceptualization. **Brenda M. Forland:** Writing – review & editing, Writing – original draft, Validation. **Timothy J. Johnson:** Writing – review & editing, Writing – original draft, Supervision, Project administration, Methodology, Investigation, Funding acquisition, Formal analysis, Data curation, Conceptualization.

## Declaration of competing interest

The authors declare that they have no known competing financial interests or personal relationships that could have appeared to influence the work reported in this paper.

## Data availability

Data will be made available on request.


### *Acknowledgements*

This work was supported by the Department of Defense's Strategic Environmental Research and Development Program (SERDP), sustainable infrastructure project SI-1649 and we thank them for their support. PNNL is operated for the U.S. Department of Energy by the Battelle Memorial Institute under contract DE-AC06-76RLO 1830.


### *Author Statement*

We have considered all issues mentioned in the reviewers' comments carefully. Changes made in response to their comments have been addressed.

## References


[1] Johnson TJ, Sams RL, Blake TA, Sharpe SW, Chu PM. Removing Aperture-induced artifacts from fourier transform infrared intensity values. Appl Opt, AO 2002;41 (15):2831–9. https://doi.org/10.1364/AO.41.002831.

[2] Sharpe SW, Johnson TJ, Sams RL, Chu PM, Rhoderick GC, Johnson PA. Gas-Phase Databases for Quantitative Infrared Spectroscopy. Appl Spectrosc 2004;58(12): 1452–61. https://doi.org/10.1366/0003702042641281.

[3] Baker TJ, Tonkyn RG, Thompson CJ, Dunlap MK, Koster van Groos PG, Thakur NA, Wilhelm MJ, Myers TL, Johnson TJ. An Infrared spectral database for gas-phase quantitation of volatile per- and polyfluoroalkyl substances (PFAS). J Quan Spectros Radiative Trans 2023;295:108420. https://doi.org/10.1016/j.jqsrt.2022.108420.

[4] Williams, S.D.; Johnson, T.J.; Sharpe, S.W.; Yavelak, V.; Oates, R.P.; Brauer, C.S. Quantitative Vapor-Phase IR Intensities and DFT Computations to Predict Absolute IR Spectra Based on Molecular Structure: I. Alkanes. Journal of Quantitative Spectroscopy and Radiative Transfer 2013, 129, 298–307. https://doi.org/10.1016/j.jqsrt.2013.07.005.

[5] Thompson CJ, Gallagher NB, Hughey KD, Dunlap MK, Myers TL, Johnson TJ. An Interactive spectral analysis tool for chemical identification and quantification of gas-phase species in complex spectra. Appl Spectrosc 2023;77(6):557–68. https://doi.org/10.1177/00037028231169304.

[6] Lindenmaier R, Scharko NK, Tonkyn RG, Nguyen KT, Williams SD, Johnson TJ. Improved assignments of the vibrational fundamental modes of ortho-, meta-, and para-xylene using gas- and liquid-phase infrared and Raman spectra combined with ab initio calculations: quantitative gas-phase infrared Spectra for Detection. J Mol Struct 2017;1149:332–51. https://doi.org/10.1016/j.molstruc.2017.07.053.

[7] Elkhazraji A, Sy M, Mhanna M, Aldhawyan J, Khaled Shakfa M, Farooq A. Selective BTEX detection using laser absorption spectroscopy in the CH bending mode region. Exp Therm Fluid Sci 2024;151:111090. https://doi.org/10.1016/j.expthermflusci.2023.111090.

[8] Van Hoomissen D, Papadimitriou VC, Burkholder JB. Low frequency (<500 Cm−1) contribution to greenhouse gas radiative efficiency. Mol Phys 2023:e2273412. https://doi.org/10.1080/00268976.2023.2273412. 0 (0).

[9] Mhanna M, Sy M, Elkhazraji A, Farooq A. A Laser-based sensor for selective detection of benzene, acetylene, and carbon dioxide in the fingerprint region. Appl Phys B 2023;129(9):139. https://doi.org/10.1007/s00340-023-08083-y.

[10] Klingbeil AE, Jeffries JB, Hanson RK. Temperature-dependent MID-IR absorption spectra of gaseous hydrocarbons. J Quan Spectros Radiative Trans 2007;107(3): 407–20. https://doi.org/10.1016/j.jqsrt.2007.03.004.

[11] Burling IR, Yokelson RJ, Griffith DWT, Johnson TJ, Veres P, Roberts JM, Warneke C, Urbanski SP, Reardon J, Weise DR, Hao WM, de Gouw J. Laboratory measurements of trace gas emissions from biomass burning of fuel types from the southeastern and southwestern United States. Atmos Chem Phys 2010;10(22): 11115–30. https://doi.org/10.5194/acp-10-11115-2010.

[12] Johnson TJ, Profeta LTM, Sams RL, Griffith DWT, Yokelson RL. An Infrared spectral database for detection of gases emitted by biomass burning. Vib Spectrosc 2010;53(1):97–102. https://doi.org/10.1016/j.vibspec.2010.02.010.

[13] Weise DR, Palarea-Albaladejo J, Johnson TJ, Jung H. Analyzing wildland fire smoke emissions data using compositional data techniques. J Geophys Res: Atmospheres 2020;125(6). https://doi.org/10.1029/2019JD032128. e2019JD032128.

[14] Pinkowski NH, Cassady SJ, Davidson DF, Hanson RK. Spectroscopic inference of alkane, alkene, and aromatic formation during high-temperature JP8, JP5, and Jet-A pyrolysis. Fuel 2020;269:117420. https://doi.org/10.1016/j.fuel.2020.117420.

[15] Gierczak T, Papanastasiou DK, Burkholder JB. Reaction of Cl atom with C-C5F8 and c-C5HF7: relative and absolute measurements of rate coefficients and identification of degradation products. J Phys Chem A 2022;126(42):7737–49. https://doi.org/10.1021/acs.jpca.2c05041.

[16] You Y, Staebler RM, Moussa SG, Su Y, Munoz T, Stroud C, Zhang J, Moran MD. Long-path measurements of pollutants and micrometeorology over highway 401 in Toronto. Atmos Chem Phys 2017;17(22):14119–43. https://doi.org/10.5194/acp-17-14119-2017.

[17] Johnson TJ, Hughey KD, Blake TA, Sharpe SW, Myers TanyaL, Sams RL. Confirmation of PNNL Quantitative Infrared Cross-Sections for Isobutane. J Phys Chem A 2021;125(17):3793–801. https://doi.org/10.1021/acs.jpca.1c01933.

[18] Johnson TJ, Disselkamp RS, Su Y-F, Fellows RJ, Alexander ML, Driver CJ. Gas-Phase Hydrolysis of SOCl2 at 297 and 309 K: Implications for Its Atmospheric Fate. J Phys Chem A 2003;107(32):6183–90. https://doi.org/10.1021/jp022090v.

[19] Nelson GO, Griggs KS. Precision Dynamic Method for Producing Known Concentrations of Gas and Solvent Vapor in Air. Review of Scientific Instruments 1968;39(6):927–8. https://doi.org/10.1063/1.1683545.

[20] Nelson GO, Hodgkins DJ. Respirator Cartridge Efficiency Studies. II. Preparation of Test Atmospheres. Am Ind Hyg Assoc J 1972;33(2):110–6. https://doi.org/10.1080/0002889728506617.

[21] Sharpe SW, Johnson TJ, Chu PM, Kleimeyer J, Rowland B, Gardner PJ. Quantitative Infrared Spectra of Vapor Phase Chemical Agents. Richland, WA (US): Pacific Northwest National Lab.; 2003. PNNL-SA-40930, https://www.osti.gov/biblio/15007898 (accessed 2023-11-15).

[22] Johnson TJ, Sharpe SW, Covert MA. Disseminator for rapid, selectable, and quantitative delivery of low and semivolatile liquid species to the vapor phase. Review of Scientific Instruments 2006;77(9):094103. https://doi.org/10.1063/1.2349298.

[23] Johnson TJ, Sams RL, Burton SD, Blake TA. Absolute integrated intensities of vapor-phase hydrogen peroxide (H2O2) in the mid-infrared at atmospheric pressure. Anal Bioanal Chem 2009;395(2):377–86. https://doi.org/10.1007/s00216-009-2805-x.

[24] Akagi SK, Yokelson RJ, Burling IR, Meinardi S, Simpson I, Blake DR, McMeeking GR, Sullivan A, Lee T, Kreidenweis S, Urbanski S, Reardon J, Griffith DWT, Johnson TJ, Weise DR. Measurements of reactive trace gases and variable $O_3$ formation rates in some south carolina biomass burning plumes. Atmos Chem Phys 2013;13(3):1141–65. https://doi.org/10.5194/acp-13-1141-2013.

[25] Pimentel GC, McClellan AL. The infrared spectra of naphthalene crystals, vapor, and solutions. J Chem Phys 1952;20(2):270–7. https://doi.org/10.1063/1.1700390.

[26] Avilés Moreno JR, Partal Ureña F, López González JJ. Hydrogen bonding network in a chiral alcohol: (1R,2S,5R-−)-Menthol. conformational preference studied by IR–Raman–VCD spectroscopies and quantum chemical calculations. Struct Chem 2013;24(2):671–80. https://doi.org/10.1007/s11224-012-0118-8.

[27] Friedel RA. Infrared spectra of phenols. J Am Chem Soc 1951;73(6):2881–4. https://doi.org/10.1021/ja01150a135.

[28] Longhi G, Abbate S, Gangemi R, Giorgio E, Rosini CFenchone. Camphor, 2-methylenefenchone and 2-methylenecamphor: a vibrational circular dichroism study. J Phys Chem A 2006;110(15):4958–68. https://doi.org/10.1021/jp057178y.

[29] King SST. Application of infrared fourier transform spectroscopy to analysis of micro samples. J Agric Food Chem 1973;21(4):526–30. https://doi.org/10.1021/jf60188a002.

[30] Kubo S, Kadla JF. Hydrogen bonding in lignin: a fourier transform infrared model compound study. Biomacromolecules 2005;6(5):2815–21. https://doi.org/10.1021/bm050288q.

[31] Wentink Jr T. Triatomic linear molecules containing carbon and oxygen, sulfur, selenium, or tellurium. I. vibrational spectra of CS2, CSe2, SCSe, and SCTe. J Chem Phys 1958;29(1):188–200. https://doi.org/10.1063/1.1744421.

[32] Cané E, Miani A, Palmieri P, Tarroni R, Trombetti A. The gas-phase infrared spectra of phenanthrene-H10 and phenanthrene-D10. Spectrochimica Acta Part A: Mol Biomol Spectrosc 1997;53(11):1839–51. https://doi.org/10.1016/S1386-1425(97)00103-0.

[33] Cané E, Puzzarini C, Tarroni R, Trombetti A. Gas-Phase IR spectrum of 1-azaindolizine: scaled quantum mechanical force field and spectrum assignment. J. Chem. Soc., Faraday Trans. 1995;91(21):3741–6. https://doi.org/10.1039/FT9959103741.

[34] Das P, Manogaran S, Arunan E, Das PK. Infrared spectra of dimethylquinolines in the gas phase: experiment and theory. J Phys Chem A 2010;114(32):8351–8. https://doi.org/10.1021/jp1056896.

[35] Brauer CS, Blake TA, Guenther AB, Sharpe SW, Sams RL, Johnson TJ. Quantitative infrared absorption cross sections of isoprene for atmospheric measurements. Atmos Meas Tech 2014;7(11):3839–47. https://doi.org/10.5194/amt-7-3839-2014.

[36] Lindenmaier R, Williams SD, Sams RL, Johnson TJ. Quantitative infrared absorption spectra and vibrational assignments of crotonaldehyde and methyl vinyl ketone using gas-phase mid-infrared, far-infrared, and liquid raman spectra: S-CIS vs s-trans composition confirmed via temperature studies and Ab initio methods. J Phys Chem A 2017;121(6):1195–212. https://doi.org/10.1021/acs.jpca.6b10872.

[37] Johnson TJ, Diaz E, Hughey KD, Myers TL, Blake TA, Dohnalkova AC, Burton SD. Infrared optical constants from pressed pellets of powders: i. improved n and k values of (NH4)2SO4 from single-angle reflectance. Appl Spectrosc 2020;74(8):851–67. https://doi.org/10.1177/0003702820930009.

[38] Johnson TJ, Baker TJ, Bradley AM, Yokosuk MO, Myers TL. Twice-modulated light in fourier transform infrared (FT-IR) spectrometers from reflective samples: avoiding distorted intensity values. Appl. Spectrosc., AS 2022;76(5):620–4. https://doi.org/10.1364/AS.76.000620.

[39] Karlovets EV, Gordon IE, Hashemi R, Kochanov RV, Hargreaves RJ, Rothman LS. Addition of the line list for carbon disulfide to the HITRAN database: line positions, intensities, and half-widths of the 12C32S2, 32S12C34S, 32S12C33S, and 13C32S2 Isotopologues. J Quant Spectros Radiative Trans 2021;258:107275. https://doi.org/10.1016/j.jqsrt.2020.107275.

[40] Xu SL, Mcdowell RS, Sharpe SW, Krohn BJ. Rovibrational Spectroscopy of C35Cl4. J Mol Spectrosc 1995;173(2):431–41. https://doi.org/10.1006/jmsp.1995.1246.

[41] Herzberg G. Molecular Spectra and Molecular Structure /2, Infrared And Raman Spectra of Polyatomic Molecules. Malabar, Fla: Krieger; 1991. Repr. ed. with corr.

[42] Taylor, J. Introduction to Error Analysis, the Study of Uncertainties in Physical Measurements, 2nd Edition; 1997.

[43] Myers L, Bernacki TE, Wilhelm BJ, Jensen ML, Johnson KJ, Primera-Pedrozo TM, Tonkyn OG, Smith RC, Burton SD, Bradley SM. A. influence of intermolecular interactions on the infrared complex indices of refraction for binary liquid Mixtures. Phys Chem Chem Phys 2022;24(36):22206–21. https://doi.org/10.1039/D2CP02920K.

[44] Bouř P, McCann J, Wieser H. measurement and calculation of absolute rotational strengths for camphor, α-pinene, and borneol. J Phys Chem A 1998;102(1):102–10. https://doi.org/10.1021/jp971665z.

[45] Abbate S, Burgi LF, Gangemi F, Gangemi R, Lebon F, Longhi G, Pultz VM, Lightner DA. Comparative analysis of IR and vibrational circular dichroism spectra for a series of camphor-related molecules. J Phys Chem A 2009;113(42):11390–405. https://doi.org/10.1021/jp905644d.

[46] Hidalgo, J.R.; Brandán, S.A. Vibrational Study of S(-) and R(+) Forms of Analgesic Camphor Combining DFT Calculations with Normal Internal Coordinates and SQMFF Methodology. 2020.

[47] Johnson JL, Zajac G, Baranska M, Polavarapu PL. Vibrational raman optical activity of camphor: the importance of electric-dipole—electric-quadrupole polarizability contribution. J Raman Spectros 2020;51(4):669–79. https://doi.org/10.1002/jrs.5829.

[48] Schwerdtfeger P, Kühn A, Bast R, Laerdahl JK, Faglioni F, Lazzeretti P. The vibrational spectrum of camphor from Ab initio and density functional theory and parity violation in the C–C*–CO bending mode. Chem Phys Lett 2004;383(5):496–501. https://doi.org/10.1016/j.cplett.2003.11.035.

[49] Quack M, Seyfang G, Wichmann G. Perspectives on parity violation in chiral molecules: theory, spectroscopic experiment and biomolecular homochirality. Chem Sci 2022;13(36):10598–643. https://doi.org/10.1039/D2SC01323A.

[50] Wittcoff HA, Reuben BG, Plotkin JS. Industrial Organic Chemicals. 2nd ed. New York: Wiley-Interscience; 1996.

[51] Hsu HC, Wang SJ, Ou JDY, Wong DSH. Simplification and intensification of a c5 separation process. Ind Eng Chem Res 2015;54(40):9798–804. https://doi.org/10.1021/acs.iecr.5b01705.

[52] Xu R, Jocz JN, Wiest LK, Sarngadharan SC, Milina M, Coleman JS, Iaccino LL, Pollet P, Sievers C, Liotta CL. Cyclopentadiene dimerization kinetics in the presence of c5 alkenes and alkadienes. Ind Eng Chem Res 2019;58(50):22516–25. https://doi.org/10.1021/acs.iecr.9b04018.

[53] Gao S, Simon SL. The reaction kinetics of cyclopentadiene dimerization using differential scanning calorimetry: experiments and modelling. Thermochim Acta 2014;589:241–6. https://doi.org/10.1016/j.tca.2014.05.031.

[54] Gallinella E, Fortunato B, Mirone P. Infrared and Raman spectra and vibrational assignment of cyclopentadiene. J Mol Spectrosc 1967;24(1):345–62. https://doi.org/10.1016/0022-2852(67)90097-5.

[55] Tjahjono AM, Feng G, Hermanto MW, Cechao F, Garland M. Combining *in Situ* FTIR spectroscopy, BTEM analysis, bulk density measurements and DFT for two diels–alder reactions. a general approach for partial molar volume and reaction volume analyses. RSC Adv 2014;4(42):22194–204. https://doi.org/10.1039/C3RA47057A.

[56] Schaubroeck D, Brughmans S, Vercaemst C, Schaubroeck J, Verpoort F. Qualitative FT-Raman investigation of the ring opening metathesis polymerization of dicyclopentadiene. J Mol Catal A: Chem 2006;254(1):180–5. https://doi.org/10.1016/j.molcata.2006.01.074.

[57] Cuisset A, Coeur C, Mouret G, Ahmad W, Tomas A, Pirali O. Infrared spectroscopy of methoxyphenols involved as atmospheric secondary organic aerosol precursors: gas-phase vibrational cross-sections. J Quan Spectros Radiative Trans 2016;179:51–8. https://doi.org/10.1016/j.jqsrt.2016.03.020.

[58] Lampert H, Mikenda W, Karpfen A. Molecular geometries and vibrational spectra of phenol, benzaldehyde, and salicylaldehyde: experimental versus quantum chemical data. J Phys Chem A 1997;101(12):2254–63. https://doi.org/10.1021/jp962933g.

[59] Rospenk M, Leroux N, Zeegers-Huyskens Th. Assignment of the vibrations in the near-infrared spectra of phenol–OH(OD) derivatives and application to the phenol–pyrazine complex. J Mol Spectrosc 1997;183(2):245–9. https://doi.org/10.1006/jmsp.1997.7284.

[60] Kjaergaard HG, Henry BR. Spectroscopic investigation of subtle CH-bond changes between solid and vapor phase naphthalene. J Phys Chem 1996;100(12):4749–54. https://doi.org/10.1021/jp9523130.

[61] Kochanov RV, Gordon IE, Rothman LS, Shine KP, Sharpe SW, Johnson TJ, Wallington TJ, Harrison JJ, Bernath PF, Birk M, Wagner G, Le Bris K, Bravo I, Hill C. Infrared absorption cross-sections in HITRAN2016 and beyond: expansion for climate, environment, and atmospheric applications. J Quan Spectros Radiative Trans 2019;238:106708. https://doi.org/10.1016/j.jqsrt.2019.106708.

[62] Wilhelm MJ, Johnson TJ, Myers TL. Disentangling the confounding spectroscopy of C1 molecules: without symmetry as a guide, everything is allowed. AIP Adv 2023;13(5):055133. https://doi.org/10.1063/5.0155054.

[63] Forland BM, Hughey KD, Wilhelm MJ, Williams ON, Cappello BF, Gaspar CL, Myers TL, Sharpe SW, Johnson TJ. Optimal spectral resolution for infrared studies of solids and liquids. Appl Spectrosc 2024.

[64] Liu N, Zhou S, Zhang L, Yu B, Fischer H, Ren W, Li J. Standoff detection of VOCs using external cavity quantum cascade laser spectroscopy. Laser Phys Lett 2018;15(8):085701. https://doi.org/10.1088/1612-202X/aac356.

[65] Myers TL, Tonkyn RG, Danby TO, Taubman MS, Bernacki BE, Birnbaum JC, Sharpe SW, Johnson TJ. Accurate measurement of the optical constants n and k for a series of 57 inorganic and organic liquids for optical modeling and detection. Appl Spectrosc 2018;72(4):535–50. https://doi.org/10.1177/0003702817742848.

[66] Pushp M, Brackmann C, Davidsson K. Infrared spectroscopy for online measurement of tars, water, and permanent gases in biomass gasification. Appl Spectrosc 2021;75(6):690–7. https://doi.org/10.1177/0003702821991891.

[67] Etzkorn T, Klotz B, Sørensen S, Patroescu IV, Barnes I, Becker KH, Platt U. Gas-Phase absorption cross sections of 24 monocyclic aromatic hydrocarbons in the UV and IR spectral ranges. Atmos Environ 1999;33(4):525–40. https://doi.org/10.1016/S1352-2310(98)00289-1.

[68] Johnson TJ, Sharpe SW, Covert MAErratum. A disseminator for rapid, selectable, and quantitative delivery of low- and semi-volatile liquid species to the vapor phase. Rev Sci Instrum 2007;78(1):019902. https://doi.org/10.1063/1.2424436.

[69] Keens, A.; Simon, A. Correction of non-linearities in detectors in fourier transform spectroscopy. US4927269A, May 22, 1990. https://patents.google.com/patent/US4927269A/en (accessed 2023-11-15).

[70] Hanst, P.L. QAsoft Software. https://ftir.com/html/qasoft_software.html.

[71] Standards. https://www.midac.com/standards.html.

[72] Jacquinet-Husson N, Scott NA, Chédin A, Crépeau L, Armante R, Capelle V, Orphal J, Coustenis A, Boonne C, Poulet-Crovisier N, Barbe A, Birk M, Brown LR, Camy-Peyret C, Claveau C, Chance K, Christidis N, Clerbaux C, Coheur PF, Dana V, Daumont L, De Backer-Barilly MR, Di Lonardo G, Flaud JM, Goldman A, Hamdouni A, Hess M, Hurley MD, Jacquemart D, Kleiner I, Köpke P, Mandin JY, Massie S, Mikhailenko S, Nemtchinov V, Nikitin A, Newnham D, Perrin A, Perevalov VI, Pinnock S, Régalia-Jarlot L, Rinsland CP, Rublev A, Schreier F, Schult L, Smith KM, Tashkun SA, Teffo JL, Toth RA, Tyuterev VlG, Vander Auwera J, Varanasi P, Wagner G. The GEISA Spectroscopic database: current and future archive for earth and planetary atmosphere studies. J. Quan. Spectros.

Radiative Transfer 2008;109(6):1043–59. https://doi.org/10.1016/j.jqsrt.2007.12.015.
[73] Scharko NK, Oeck AM, Myers TL, Tonkyn RG, Banach CA, Baker SP, Lincoln EN, Chong J, Corcoran BM, Burke GM, Ottmar RD, Restaino JC, Weise DR, Johnson TJ. Gas-phase pyrolysis products emitted by prescribed fires in pine forests with a shrub understory in the southeastern united states. Atmos Chem Phys 2019;19(15):9681–98. https://doi.org/10.5194/acp-19-9681-2019.
[74] Scharko NK, Oeck AM, Tonkyn RG, Baker SP, Lincoln EN, Chong J, Corcoran BM, Burke GM, Weise DR, Myers TL, Banach CA, Griffith DWT, Johnson TJ. Identification of gas-phase pyrolysis products in a prescribed fire: first detections using infrared spectroscopy for naphthalene, methyl nitrite, allene, acrolein and acetaldehyde. Atmos Meas Tech 2019;12(1):763–76. https://doi.org/10.5194/amt-12-763-2019.
[75] Pouchert, C.J. Aldrich Library of FT-IR Spectra: vapor Phase, Volume 3; 2007.
[76] NIST Standard Reference Database 35. NIST 2010, https://www.nist.gov/srd/nist-standard-reference-database-35.
[77] Roberts JM, Veres P, Warneke C, Neuman JA, Washenfelder RA, Brown SS, Baasandorj M, Burkholder JB, Burling IR, Johnson TJ, Yokelson RJ, de Gouw J. Measurement of HONO, HNCO, and other inorganic acids by negative-ion proton-transfer chemical-ionization mass spectrometry (NI-PT-CIMS): application to biomass burning Emissions. Atmos Meas Tech 2010;3(4):981–90. https://doi.org/10.5194/amt-3-981-2010.
[78] Akagi SK, Burling IR, Mendoza A, Johnson TJ, Cameron M, Griffith DWT, Paton-Walsh C, Weise DR, Reardon J, Yokelson RJ. Field measurements of trace gases emitted by prescribed fires in southeastern us pine forests using an open-path FTIR system. Atmos Chem Phys 2014;14(1):199–215. https://doi.org/10.5194/acp-14-199-2014.
[79] Weise DR, Johnson TJ, Reardon J. Particulate and trace gas emissions from prescribed burns in southeastern U.S. fuel types: summary of a 5-year project. Fire Saf J 2015;74:71–81. https://doi.org/10.1016/j.firesaf.2015.02.016.
[80] Yee LD, Kautzman KE, Loza CL, Schilling KA, Coggon MM, Chhabra PS, Chan MN, Chan AWH, Hersey SP, Crounse JD, Wennberg PO, Flagan RC, Seinfeld JH. Secondary organic aerosol formation from biomass burning intermediates: phenol and methoxyphenols. Atmos Chem Phys 2013;13(16):8019–43. https://doi.org/10.5194/acp-13-8019-2013.
[81] Laskin A, Smith JS, Laskin J. Molecular characterization of nitrogen-containing organic compounds in biomass burning aerosols using high-resolution mass spectrometry. Environ Sci Technol 2009;43(10):3764–71. https://doi.org/10.1021/es803456n.
[82] Hu Y, Odman MT, Chang ME, Jackson W, Lee S, Edgerton ES, Baumann K, Russell AG. Simulation of air quality impacts from prescribed fires on an urban area. Environ Sci Technol 2008;42(10):3676–82. https://doi.org/10.1021/es071703k.
[83] Lee S, Kim HK, Yan B, Cobb CE, Hennigan C, Nichols S, Chamber M, Edgerton ES, Jansen JJ, Hu Y, Zheng M, Weber RJ, Russell AG. Diagnosis of aged prescribed burning plumes impacting an urban area. Environ Sci Technol 2008;42(5):1438–44. https://doi.org/10.1021/es7023059.
[84] Yan B, Zheng M, Hu YT, Lee S, Kim HK, Russell AG. Organic composition of carbonaceous aerosols in an aged prescribed fire plume. Atmos Chem Phys 2008;8(21):6381–94. https://doi.org/10.5194/acp-8-6381-2008.
[85] Mar Quesada-Moreno M, Virgili A, Monteagudo E, M Claramunt R, Ramón Avilés-Moreno J, Jesús López-González J, Alkorta I, Elguero J. A vibrational circular dichroism (VCD) methodology for the measurement of enantiomeric excess in chiral compounds in the solid phase and for the complementary use of NMR and VCD techniques in solution: the camphor case. Analyst 2018;143(6):1406–16. https://doi.org/10.1039/C7AN01855J.